



HAL
open science

MAVEN observation of an obliquely propagating low-frequency wave upstream of Mars

Suranga Ruhunusiri, J. S. Halekas, J. E. P. Connerney, J. R. Espley, J. P. Mcfadden, C. Mazelle, D. Brain, G. Collinson, Y. Harada, D. E. Larson, et al.

► **To cite this version:**

Suranga Ruhunusiri, J. S. Halekas, J. E. P. Connerney, J. R. Espley, J. P. Mcfadden, et al.. MAVEN observation of an obliquely propagating low-frequency wave upstream of Mars. *Journal of Geophysical Research Space Physics*, 2016, 121, pp.2374-2389. 10.1002/2015JA022306 . insu-03670532

HAL Id: insu-03670532

<https://insu.hal.science/insu-03670532>

Submitted on 17 May 2022

HAL is a multi-disciplinary open access archive for the deposit and dissemination of scientific research documents, whether they are published or not. The documents may come from teaching and research institutions in France or abroad, or from public or private research centers.

L'archive ouverte pluridisciplinaire **HAL**, est destinée au dépôt et à la diffusion de documents scientifiques de niveau recherche, publiés ou non, émanant des établissements d'enseignement et de recherche français ou étrangers, des laboratoires publics ou privés.

RESEARCH ARTICLE

10.1002/2015JA022306

MAVEN observation of an obliquely propagating low-frequency wave upstream of Mars

Suranga Ruhunusiri¹, J. S. Halekas¹, J. E. P. Connerney², J. R. Espley², J. P. McFadden³, C. Mazelle^{4,5}, D. Brain⁶, G. Collinson², Y. Harada³, D. E. Larson³, D. L. Mitchell³, R. Livi³, and B. M. Jakosky⁶¹Department of Physics and Astronomy, The University of Iowa, Iowa City, Iowa, USA, ²NASA Goddard Space Flight Center, Greenbelt, Maryland, USA, ³Space Sciences Laboratory, University of California, Berkeley, California, USA, ⁴CNRS, IRAP, Toulouse, France, ⁵University Paul Sabatier, Toulouse, France, ⁶Laboratory for Atmospheric and Space Physics, University of Colorado Boulder, Boulder, Colorado, USA

Key Points:

- MAVEN observes a large amplitude low-frequency wave and a non-solar wind component upstream of Mars
- The wave is excited by newly born pickup protons or bow shock reflected solar wind protons
- The non-solar wind component does not generate the wave, but merely perturbed by it

Correspondence to:

S. Ruhunusiri,
suranga-ruhunusiri@uiowa.edu

Citation:

Ruhunusiri, S., et al. (2016), MAVEN observation of an obliquely propagating low-frequency wave upstream of Mars, *J. Geophys. Res. Space Physics*, 121, 2374–2389, doi:10.1002/2015JA022306.

Received 23 DEC 2015

Accepted 25 FEB 2016

Accepted article online 27 FEB 2016

Published online 29 MAR 2016

Abstract We report Mars Atmosphere and Volatile Evolution (MAVEN) mission observations of a large amplitude low-frequency plasma wave that propagated oblique to the ambient magnetic field upstream of Mars along with a non-solar-wind plasma component that had a flow velocity perpendicular to the magnetic field. We consider nine possibilities for this wave that include various combinations of its propagation direction, polarization in the solar wind frame, and ion source responsible for its generation. Using the observed wave parameters and the measured plasma parameters as constraints, we uniquely identify the wave by systematically discarding these possibilities. We determine that the wave is a right-hand polarized wave that propagated upstream in the solar wind frame. We find two possibilities for the ion source that can be responsible for this wave generation. They are either newly born pickup protons or reflected solar wind protons from the bow shock. We determine that the observed non-solar-wind component is not responsible for the wave generation, and it is likely that the non-solar-wind component was merely perturbed by the passage of the wave.

1. Introduction

The objective of this paper is to interpret the type and the source for a low-frequency wave observed upstream of Mars by Mars Atmosphere and Volatile Evolution (MAVEN). This wave observation was unique because of several interesting wave properties and corresponding upstream parameters. In particular, the wave had very large fluctuations in ion density and magnetic field that were correlated and the wave propagated oblique to the ambient magnetic field. The ambient magnetic field during this interval was pointing upstream, nearly antiparallel to the solar wind flow. A low-density non-solar-wind plasma component was also observed simultaneously with the wave, and it was flowing oblique to the ambient magnetic field. In this paper, we answer the following questions regarding the wave:

1. What is the polarization of the wave in the solar wind frame (left or right handed)?
2. What is the propagation direction of the wave in the solar wind frame (upstream or downstream)?
3. What is the ion source responsible for the wave generation? For example, can the observed non-solar-wind component be responsible for the wave generation? Or is the wave generated by newly born pickup ions or bow shock reflected solar wind ions?

Planetary upstream regions, in general, are home to a variety of ion populations such as solar wind pickup ions, bow shock reflected solar wind ions, bow shock reflected pickup ions, and ions leaked from the magnetosheath [Russell, 1994]. When these ion populations interact with the solar wind, they can lead to generation of low-frequency (LF) plasma waves via resonance, usually with a frequency near the ion gyrofrequency [Russell, 1994]. Upstream LF waves excited by newly born pickup ions have been observed at Mars [Russell et al., 1990] and at comets [Brinca and Tsurutani, 1987; Brinca, 1996; Le et al., 1989; Mazelle and Neubauer, 1993; Tan et al., 1993; Thorne and Tsurutani, 1987; Tsurutani and Smith, 1986; Tsurutani et al., 1987]. These pickup ions are formed by photoionization or electron impact ionization of neutrals in the exospheres of planets and comets. Pickup ion generated LF waves have also been observed near Io [Warnecke et al., 1997; Russell et al., 2003] and in the vicinity of Saturn rings [Leisner et al., 2006]. Low-frequency waves excited by bow shock reflected solar wind ions (backstreaming ions) have been observed at Mercury [Le et al., 2013], Venus [Wei et al., 2011],

Earth [Le and Russell, 1994; Russell, 1994; Hoppe et al., 1981; Hoppe and Russell, 1983], Saturn [Cattaneo et al., 1991; Orlowski et al., 1992], Jupiter [Smith et al., 1983; Goldstein et al., 1983; Tsurutani et al., 1993], Uranus [Russell et al., 1990], and Neptune [Zhang et al., 1991]. In some cases, LF upstream waves observed at Uranus and Saturn are also suggested to be excited by ions leaked from their magnetosheaths [Russell et al., 1990; Orlowski et al., 1992]. Low-frequency upstream waves that are excited by reflected ions from the moon have also been reported [Halekas et al., 2013].

At Mars, upstream proton-cyclotron-like waves have been observed by a number of spacecraft including Phobos 2 and Mars Global Surveyor [Brain et al., 2002; Bertucci et al., 2005; Delva et al., 2011; Mazelle et al., 2004; Russell et al., 2006; Wei and Russell, 2006; Wei et al., 2011; Romanelli et al., 2013; Wei et al., 2014]. Proton-cyclotron-like waves are LF waves which are left-hand polarized in the spacecraft frame, have transverse power higher than compressional power, and have frequencies near the local proton gyrofrequency. A number of statistical studies, mainly using spacecraft magnetometers, have enabled characterization of these waves at Mars [Brain et al., 2002; Wei and Russell, 2006; Romanelli et al., 2013; Wei et al., 2014]. These proton-cyclotron-like waves were found at distances as large as $4 R_M$ (Martian radii), and the wave power was found to generally decrease with distance from the planet [Wei et al., 2014]. The waves were found with a highest occurrence rate when the cone angle (the angle between the magnetic field and the solar wind flow) is 45° . However, the wave frequency, wave amplitude, and wave duration were found not to significantly vary with the cone angle [Wei et al., 2014]. Moreover, these waves at Mars were predominantly found in the positive electric field side [Wei and Russell, 2006; Wei et al., 2014].

Previous investigations suggested that these upstream proton-cyclotron-like waves at Mars are excited by the newly born pickup ions [Mazelle et al., 2004], and to date, there have been no definitive identification of LF waves associated with other ion sources such as bow shock reflected ions at Mars. Thus, if LF waves due to these other ion sources indeed do occur, it is interesting to identify them from the newly born pickup ion generated waves and to characterize their relative contributions to the upstream waves at Mars. Since wave properties for the waves generated from such different ion sources can be similar, one approach for their identification involves determining which ion source can resonate with the wave consequently leading to its generation. In doing so, we have to also consider the two possible wave polarization states in the solar wind frame (left versus right hand). Using the observed wave parameters and the measured ambient plasma parameters, we can distinguish among these possibilities for the ion sources and the wave polarization states. This is the approach that we use in our selected case study.

2. MAVEN Instruments Used for Wave and Plasma Diagnostics

We use the MAVEN Solar Wind Ion Analyzer (SWIA), SupraThermal And Thermal Ion Composition (STATIC), and Magnetometer (MAG) instruments for measuring the wave parameters and the ambient plasma conditions. SWIA is a toroidal electrostatic analyzer that measures ion fluxes and ion moments over a broad energy range from 10 eV to 25 keV with a sampling cadence of 4 s [Halekas et al., 2013]. STATIC is a toroidal electrostatic analyzer that has mass resolution capability [McFadden et al., 2015]. It makes measurements of ion populations with a cadence of 4 s. The MAG instrument is a fluxgate magnetometer that provides vector magnetic field measurements over a broad range for three axes at a sampling cadence of 32 Hz [Connerney et al., 2015]. In the solar wind, the MAG instrument measurement accuracy is 0.15 nT or a few degrees [Connerney et al., 2015]. The sampling cadences of SWIA, STATIC, and MAG, as well as their broad measurement ranges, are adequate to resolve low-frequency waves in the upstream region as demonstrated by Ruhunusiri et al. [2015]. The broad energy range of SWIA is adequate not only to resolve the solar wind but also to resolve various ion populations in the upstream region of Mars, including pickup ions and bow shock reflected ions.

3. Upstream Wave and Non-Solar-Wind Component Observations

The upstream low-frequency wave that is the focus of this study was observed by MAVEN on 29 December 2014 (Figure 1). This observation was made while the spacecraft traversed toward the magnetosheath upstream of the model-predicted bow shock location (Figure 2a). The actual bow shock location can vary from this model bow shock location. However, the complicated nature of the upstream conditions prevailed during this observation does not enable us to discern the actual bow shock location. The wave appeared quasi monochromatic during the time interval 14:30 to 14:40, and it was relatively broadband elsewhere (Figure 1i). Wave parameters for this time interval are shown in Figure 3. We will use these parameters to

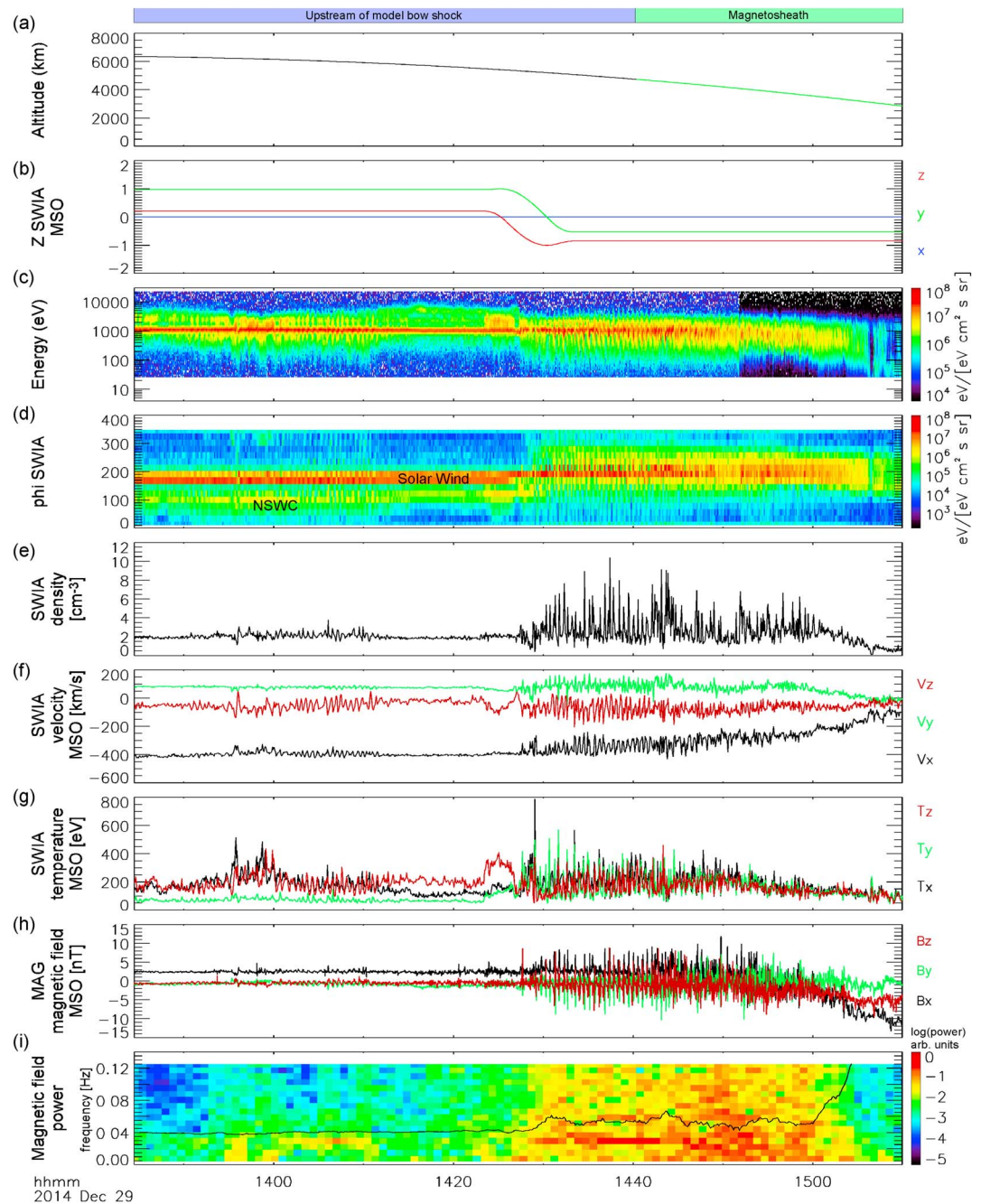


Figure 1. MAVEN SWIA and MAG observations of the upstream LF wave. (a) Spacecraft altitude. (b) SWIA Z attitude vector indicates that MAVEN was reoriented at 14:30. (c) SWIA energy spectrum. (d) SWIA phi angle spectrum (in instrument coordinates) depicts the non-solar-wind component which is directionally separated from the solar wind component. (e–g) SWIA measurements of ion moments indicate large fluctuations associated with the wave. (h) MAG measurements depict very large fluctuations in the magnetic field that are correlated with the ion density fluctuations. (i) Magnetic field power spectrum. The proton gyrofrequency is shown in black.

determine wave resonance conditions in section 4. The wave frequency (i.e., the frequency in the spacecraft frame corresponding to the maximum wave power) was 0.031 Hz, which was below the local proton gyrofrequency (0.041 Hz).

The wave had large fluctuations in the magnetic field and ion moments (Figures 1h and 1e–1g). The ion density fluctuations, in particular, were correlated with the magnetic field fluctuations and anticorrelated with the ion temperature fluctuations. These correlations were determined by a visual inspection of the time

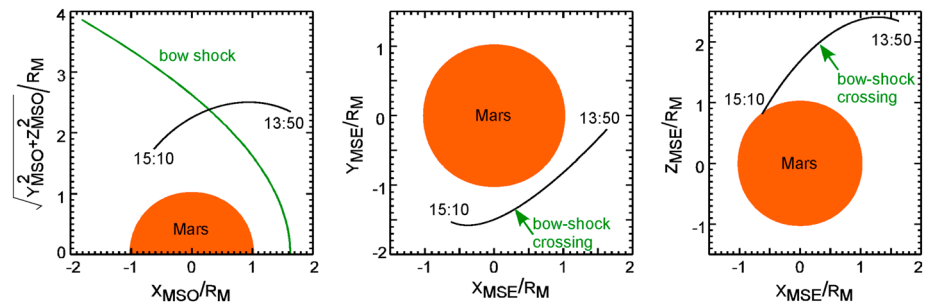


Figure 2. Different projections of MAVEN orbit during the wave observation. (a) MAVEN orbit in Mars-centered Solar Orbital (MSO) coordinates with the model bow shock from *Trotignon et al.* [2006] marked in green. (b) Orbital projection in MSE (Mars Solar Electric)-x and MSE-y coordinates. Here the MSE-x direction is oriented parallel to the solar wind velocity, while the MSE-y direction is oriented so that it is parallel to the magnetic field perpendicular to the solar wind velocity. (c) Orbital projection in MSE-x and MSE-z coordinates. Here the MSE-z direction is oriented parallel to the convection electric field. The convection electric field direction was determined using the average values of the magnetic field and the ion velocity in the upstream region. The wave was observed in the negative B hemisphere and in the positive E hemisphere.

series data. The wave was highly transverse with transverse fluctuations exceeding compressional fluctuations. In the spacecraft frame, the wave had a left-hand polarization with an ellipticity of -0.53 (Figure 3b). Minimum variance analysis revealed that the wave propagated oblique to the ambient magnetic field at an angle of 30° or 150° (Figure 3c). We obtain two values for the wave propagation angle here because the minimum variance analysis cannot uniquely determine the wave propagation direction. Similarly, we find that the wave propagation direction made an angle of 138° or 42° with respect to the solar wind velocity (Figure 3d).

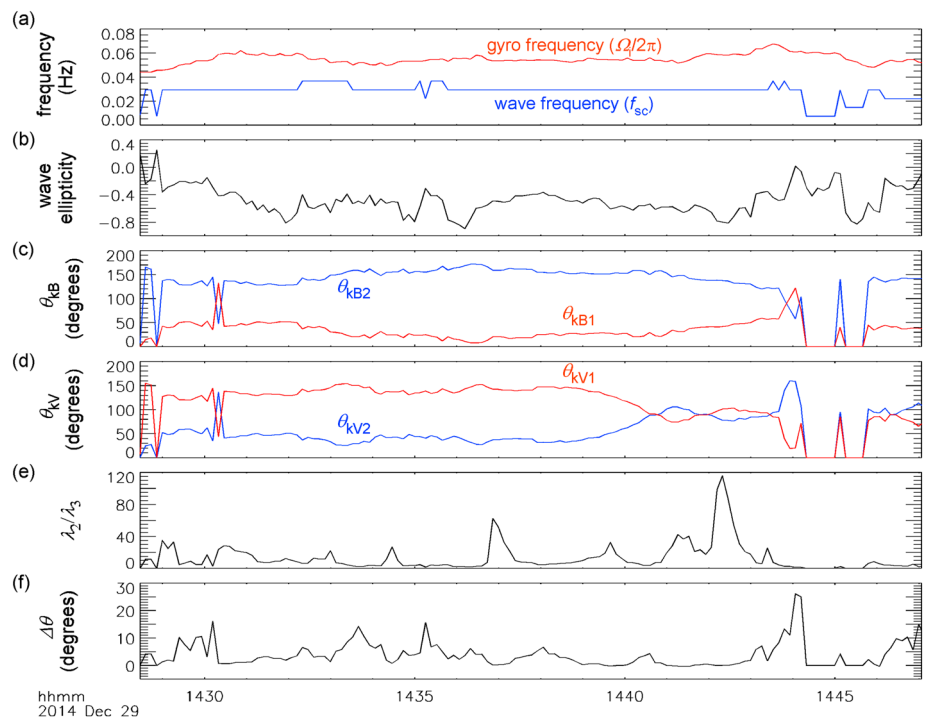


Figure 3. Wave parameters. (a) Wave frequency in the spacecraft frame f_{sc} is below the proton gyrofrequency $\Omega_i/2\pi$. (b) Wave ellipticity in the spacecraft frame indicates that it has a left-hand polarization. (c) Two values for the angle between the wave vector and the ambient magnetic field θ_{kB} computed using minimum variance analysis. (d) Two values for the angle between the wave vector and the solar wind velocity θ_{kV} . The angle values shown here in red θ_{kV1} correspond with θ_{kB1} in Figure 3c. For example, at 14:35 $\theta_{kV1} = 130^\circ$, and the corresponding angle between the wave vector and the magnetic field is $\theta_{kB1} = 30^\circ$. (e) Ratio between the intermediate and minimum eigen values, λ_2 and λ_3 , respectively. (f) Wave angle uncertainty $\Delta\theta$ computed based on *Hoppe et al.* [1981]. Averages of these parameters during the time interval 14:30–14:40, where these parameters are relatively steady, are used to determine wave resonance conditions in section 4.

Table 1. Average Wave Parameters During the Time Interval 14:30 to 14:40

Wave Parameter	Value
Angle between wave vector and magnetic field θ_{kB}	30° (150°)
Angle between wave vector and the solar wind velocity θ_{kV}	138° (42°)
Wave frequency in spacecraft frame f_{sc}	0.031 Hz
Wave angle uncertainty $\Delta\theta$	4°

To compute these wave parameters, we use 128 s time windows that are shifted by 8 s increments. Prior to performing minimum variance analysis, we bandpass filtered the magnetic field centered at the peak frequency to obtain a better estimate of the wave direction. The above stated values for angles and ellipticity are the averages for the time interval 14:30 to 14:40 for the dominant wave component (i.e., fluctuations with maximum power). These wave parameters are summarized in Table 1, and we will use them later in section 4 to determine the type of the wave and the ion source responsible for the wave generation.

In addition to the wave, we also observe a non-solar-wind plasma component (NSWC) which is directionally separated from the solar wind component. One of our objectives in this paper is to determine whether this NSWC is responsible for generation of the observed wave. The NSWC is visible in the SWIA phi angle spectrum of the ion fluxes (Figure 1d). In particular, the solar wind occupies phi angles from 150° to 210°, whereas the NSWC occupies phi angles below 150° prior to 14:30. After 14:30 this NSWC occupies phi angles greater than 210°. This change in direction is not a physical phenomenon but merely a consequence of reorientation of the SWIA field of view due to a spacecraft rotation at 14:30 as shown in Figure 1b. Two-dimensional velocity plots for this beam indicate that this beam is oblique to the magnetic field (Figure 4). We use STATIC to determine the ion composition of the NSWC, shown in Figure 5.

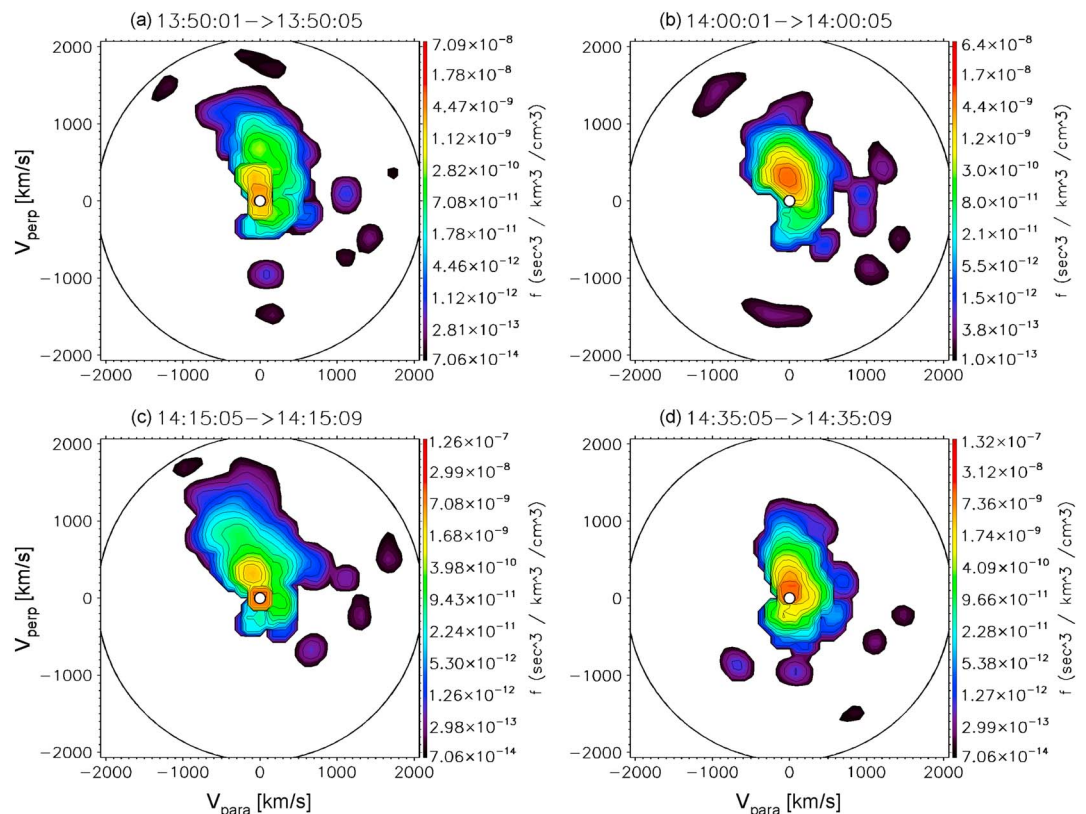


Figure 4. Two-dimensional slices of 3-D velocity distribution function for the NSWC from SWIA with respect to the magnetic field. The contributions of the solar wind component are not shown here. (a–c) Velocity distribution functions for the NSWC prior to the wave observation. (d) Velocity distribution function for a time that coincides with the wave observation. The NSWC has a bulk velocity perpendicular to the ambient magnetic field for all these cases.

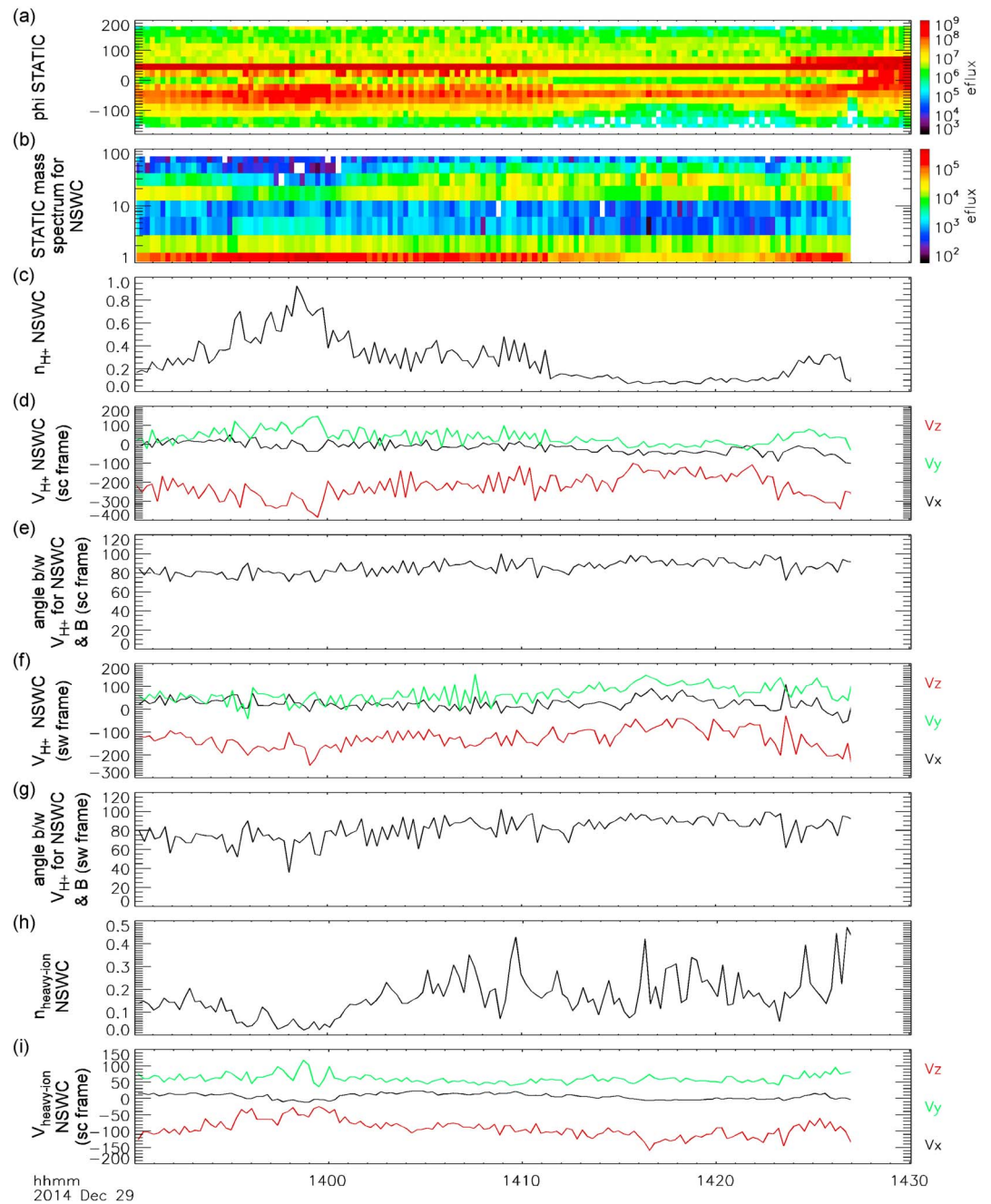


Figure 5. Non-solar-wind component parameters. (a) STATIC phi angle spectrum (in instrument coordinates) depicts the non-solar-wind component between angles -180° and 0° and the solar wind component between angles 0° and 90° . (b) STATIC mass spectrum for the NSWC component. The contributions from the solar wind component are not shown here. The NSWC component consists mainly of H^+ , but some heavy ions like O^+ are also present. (c) H^+ density for the NSWC. (d) H^+ velocity for the NSWC in the spacecraft frame. The velocity vectors are depicted in the MSO coordinate system. (e) Angle between the H^+ velocity and the magnetic field for the NSWC in the spacecraft frame. (f) H^+ velocity for the NSWC in the solar wind frame depicted in the MSO coordinate system. (g) Angle between the H^+ velocity and the magnetic field for the NSWC in the solar wind frame. (h) Heavy ion density for the NSWC. (i) Heavy ion velocity for the NSWC in the spacecraft frame shown in MSO coordinate system.

Table 2. Average Parameters for the Solar Wind and the Non-Solar Wind Components During the Time Interval 13:50 to 14:20^a

Parameter	Solar Wind Value	NSWC Value
Density (cm ⁻³)	1.8 ± 0.2 (SWIA)	0.17 ± 0.09 (SWIA) $n_{H^+} = 0.3 \pm 0.2$ (STATIC) $n_{\text{heavy ion}} = 0.15 \pm 0.08$ (STATIC)
Velocity (km/s)	441 ± 11 (SWIA)	sc frame 307 ± 74 (SWIA) $V_{H^+} = 228 \pm 63$ (STATIC) sw frame 213 ± 62 (SWIA) $V_{H^+} = 152 \pm 30$ (STATIC)
Angle between velocity and B (deg)	162 ± 5 (SWIA)	sc frame 85 ± 9 (SWIA) $\theta_{V_{H^+}B} = 84 \pm 7$ (STATIC) sw frame 81 ± 14 (SWIA) $\theta_{V_{H^+}B} = 80 \pm 12$ (STATIC)

^aHere sc frame and sw frame refer to the spacecraft frame and the solar wind frame, respectively. Standard deviation of these parameters is shown as uncertainties. Here n_{H^+} , V_{H^+} , and $\theta_{V_{H^+}B}$ are the H⁺ ion density, H⁺ ion velocity, and the angle between the H⁺ ion velocity and the magnetic field, respectively. The ion density for ions with masses between 10 to 40 amu are denoted by $n_{\text{heavy ion}}$.

Parameters for both the solar wind component and the NSWC are summarized in Table 2. The NSWC mainly consists of H⁺, but heavier ions like O⁺ are also present (Figure 5b). We compute NSWC parameters, in particular, its velocity and the angle it makes with the magnetic field in both the spacecraft frame and the solar wind frame. The solar wind frame parameters for the NSWC are required to determine whether it is responsible for generation of the wave as we describe in section 4. To convert the NSWC velocity in the spacecraft frame to the solar wind frame, we subtract the $E \times B$ drift velocity from its velocity in the spacecraft frame. Here $E = -V_{\text{sw}} \times B$, where E is the solar wind electric field, V_{sw} is the solar wind velocity, and B is the magnetic field.

4. Interpretation for the Wave

Now we will determine the ion source responsible for the generation of the observed wave, the wave polarization, and its propagation direction in the solar wind frame. In particular, we will determine that the wave is generated by either newly born pickup ions from a distant exospheric source or reflected solar wind ions from the bow shock. We will also determine that in the solar wind frame, the wave is right-hand polarized and it propagates upstream. The wave appears left-hand polarized in the spacecraft frame because of the solar wind convection. The following is a discussion of how we arrive at these conclusions.

There are two possibilities for the wave propagation direction: upstream and downstream (see Figure 6). Based on the minimum variance analysis, as described in section 3, we found that there are two possible values for the angle between the wave vector and the solar wind velocity θ_{kV} (see Table 1). The larger angle, i.e., $\theta_{kV} = 138^\circ$, corresponds to an upstream propagating wave (Figure 6a). On the other hand, the smaller angle, i.e., $\theta_{kV} = 42^\circ$, corresponds to a downstream propagating wave (Figure 6b). While the observed wave is left-hand polarized in the spacecraft frame, it can be either left- or right-hand polarized in the solar wind frame.

In addition to the observed NSWC, we consider two other ion populations that could be responsible for the generation of the wave: newly born pickup ions and specularly reflected solar wind ions from the bow shock. The above three ion populations have different velocities in the solar wind frame (Figure 7) and consequently lead to different resonance requirements. To determine whether the wave can resonate with a given ion population, in particular, requires their velocity parallel to the magnetic field. In the solar wind frame,

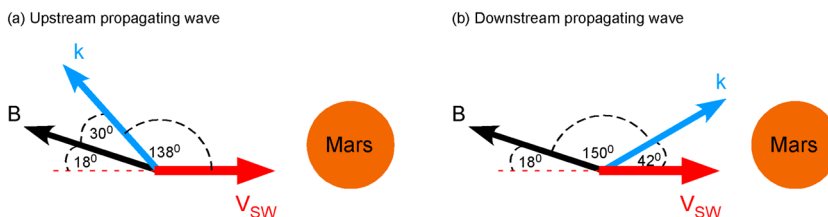


Figure 6. Interpretation for the wave propagation direction in the solar wind frame based on the observed minimum variance angles. (a) The smaller angle between that of the magnetic field and the wave vector corresponds to an upstream propagating wave. (b) The larger angle corresponds to a downstream propagating wave.

the newly born pickup ions move with a velocity equal and opposite to the solar wind velocity (Figure 7a). Since we find that $V_{sw} = 441$ km/s, the newly born pickup ion velocity parallel to the magnetic field should be $V_{sw} \cos(18) = 419$ km/s. If we assume specularly reflected solar wind ions from the bow shock, on the other hand, their velocity in the solar wind frame should depend on their reflection point from the bow shock (Figure 8). In particular, the velocity parallel to the magnetic field in the solar wind frame $V_{reflected||B}$ depends on the angle between the solar wind flow and the bow shock normal, θ_{VN} , and cone angle (Figures 7b and 8b). Here we assume that the bow shock normal N , V_{sw} , and B are coplanar. For specular reflection from a bow shock, the velocity component perpendicular to N remains unchanged, while the component parallel to N is reversed [Gosling et al., 1982]. Thus, the bow shock reflected solar wind ions have the same magnitude for the velocity as that of the solar wind ions impinging on the bow shock. The bow shock reflected solar wind ions also make the same angle to N as that of the solar wind ions. Finally, for the NSWC component, the angle between its velocity and the magnetic field is 80° (as shown in Figure 7c). So its velocity component parallel to the magnetic field is $152 \cos(80) = 26$ km/s.

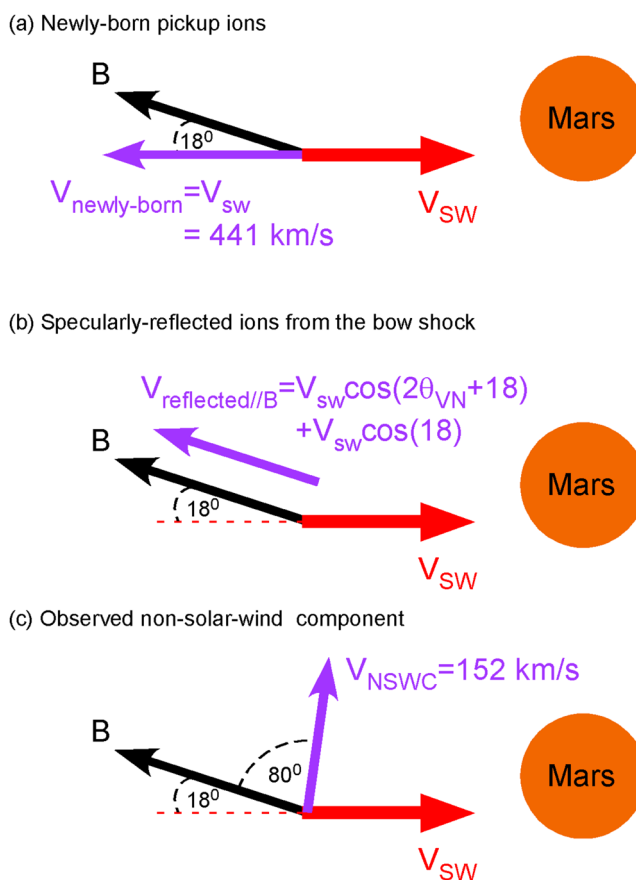


Figure 7. (a–c) Three ion populations that can be responsible for the generation of the observed wave and their velocity characteristics in the solar wind frame.

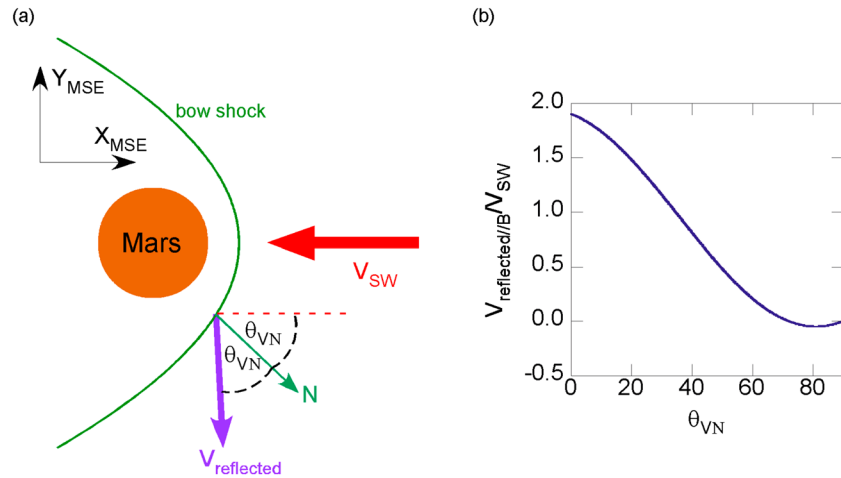


Figure 8. (a) Solar wind ion reflection geometry from the bow shock. (b) The relationship between the velocity of the bow shock reflected ions parallel to the magnetic field in the solar wind frame and the angle between the solar wind velocity and the bow shock normal N θ_{VN} .

The generation of waves with resonance with these ion populations requires that the wave polarization with respect to the ion beam should be left handed. For this to occur, the angular frequency of the wave in the solar wind frame ω_0 , the ion beam velocity parallel to the magnetic field in the solar wind frame V_b , and the local proton gyrofrequency Ω_i should be related as

$$\omega_0 - k \cdot V_b \pm \Omega_i = 0. \tag{1}$$

Here k is the wave vector and plus and minus signs are associated with right- and left-hand polarized waves, respectively. The solar wind convection leads the wave frequency to be Doppler shifted to

$$\omega_{sc} = \omega_0 + k \cdot V_{sw}. \tag{2}$$

where ω_{sc} is the frequency of the wave in the spacecraft frame.

Now we consider a total of nine possibilities (three subgroups with three each) for the wave to determine three aspects for the wave: the ion population responsible for wave generation, the wave propagation direction, and its polarization in the solar wind frame. Specifically, we consider three cases for the wave for a given ion population. To restrict among these possibilities, we require that the wave be able to resonate with the ion beam, the wave polarization is left handed in the spacecraft frame, and that ω_0 and k are positive.

4.1. Newly Born Pickup Ion Generated Waves

Here we will refer to the right- and left-hand polarized waves as RH and LH waves, respectively. The three cases for the wave that we consider here are upstream propagating RH wave (Figure 9a), upstream propagating LH wave (Figure 9b), and downstream propagating LH wave (Figure 9c). We do not consider the downstream propagating RH wave because it would be observed in the spacecraft frame as a RH wave and not a LH wave. Thus, we will also omit this downward propagating RH wave when considering the other two ion populations in sections 4.2 and 4.3. Now we will consider each of these three cases one at a time.

For the upstream propagating RH wave (Figure 9a), resonance with the newly born pickup ions requires that the wave should be left-hand polarized in the ion frame. For this to occur the wave phase velocity parallel to the magnetic field must be smaller than the ion beam velocity parallel to the magnetic field, i.e., $\omega_0/k < k_{unit} \cdot V_b$, where k_{unit} is the unit wave vector. Since for the newly born pickup ions $V_b = 441 \cos(18)$ km/s, the phase velocity $V_{ph} = \omega_0/k$ must be smaller than $V_b \cos(30) = 363$ km/s. For the wave to be left-hand polarized in the spacecraft frame, on the other hand, requires that the wave phase velocity antiparallel to the solar wind velocity must be smaller than the solar wind velocity, i.e., $\omega_0/k < -k_{unit} \cdot V_{sw}$. Thus, V_{ph} must be smaller than $-V_{sw} \cos(138) = 328$ km/s. Thus, in order for the wave to be resonant with the newly born pickup ions and to be perceived in the spacecraft frame as a left-hand polarized wave require that $V_{ph} < 328$ km/s.

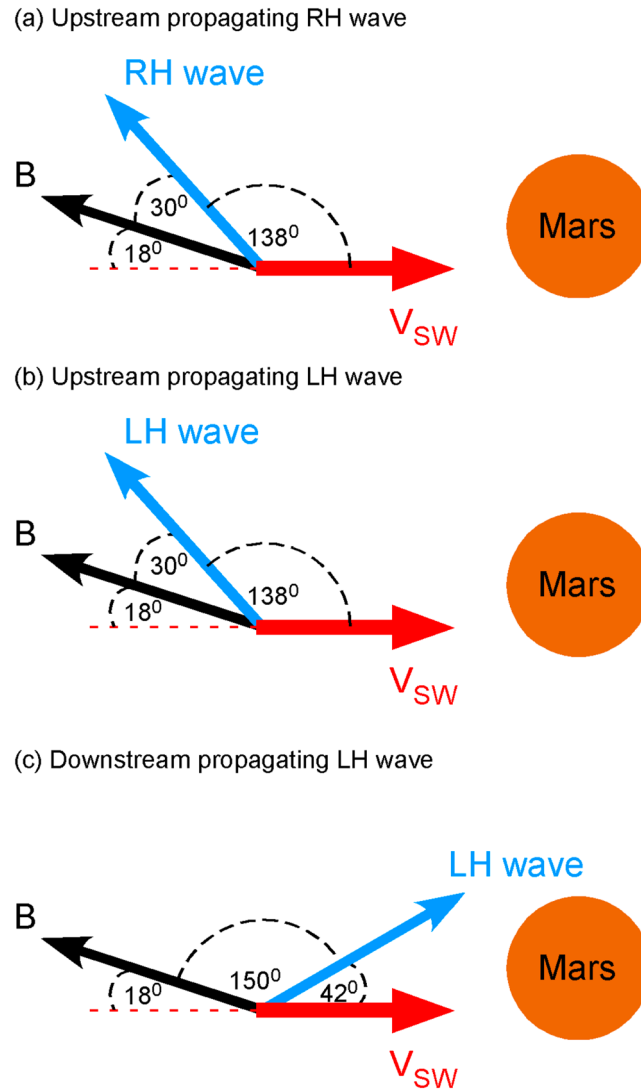


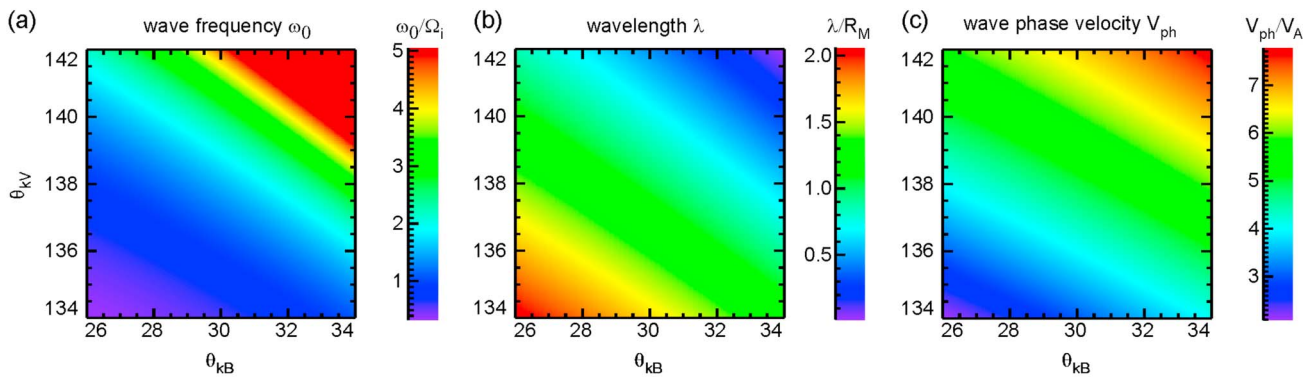
Figure 9. (a–c) Three possibilities for the wave that can resonate with the ion populations that we consider and that will be perceived in the spacecraft as a left-hand polarized wave.

Now we use equations (1) and (2) to find the wave frequency $f_0 = \omega_0/(2\pi)$ and k subjected to three constraints: $V_{ph} < 328$ km/s, and f_0 and k should be positive. Here we find a valid solution with $f_0 = 0.07$ Hz, $\lambda = 0.9 R_M$, and $V_{ph} = 232$ km/s, where R_M is the Mars radius. Thus, one possibility for our observed wave is the newly born pickup ion excited right-hand polarized wave that propagates upstream.

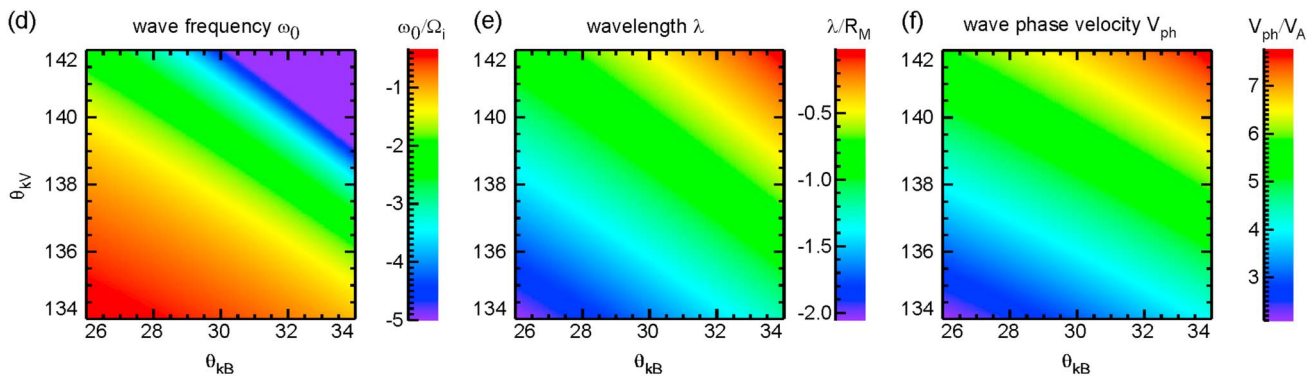
For the upstream propagating LH wave (Figure 9b), the constraints for the wave phase velocity are different from the previous case. In particular, to resonate with the ion beam requires that the wave phase velocity parallel to the magnetic field must be larger than the ion beam velocity parallel to the magnetic field, i.e., $\omega_0/k > k_{unit} \cdot V_b$. For the wave to be left-hand polarized in the spacecraft frame requires that the wave phase velocity antiparallel to the solar wind velocity must be larger than the solar wind velocity, i.e., $\omega_0/k > -k_{unit} \cdot V_{sw}$. Thus, the constraints for this wave to be the observed wave are $V_{ph} > 363$ km/s, and f_0 and k should be positive. Using equations (1) and (2) as before, we find that $f_0 = -0.07$ Hz, $\lambda = -0.9 R_M$, and $V_{ph} = 294$ km/s. Since we obtain negative values for f_0 and k , and V_{ph} is not larger than 363 km/s, this is not a valid solution. Thus, the observed wave cannot be a newly born pickup ion generated left-hand polarized wave that propagates upstream.

Finally, for the newly born pickup ion generated waves, we consider the downstream propagating LH wave (Figure 9c). This wave is perceived in both the ion frame and the spacecraft frame as a left-hand polarized

Upstream propagating RH wave parameters



Upstream propagating LH wave parameters



Downstream propagating LH wave parameters

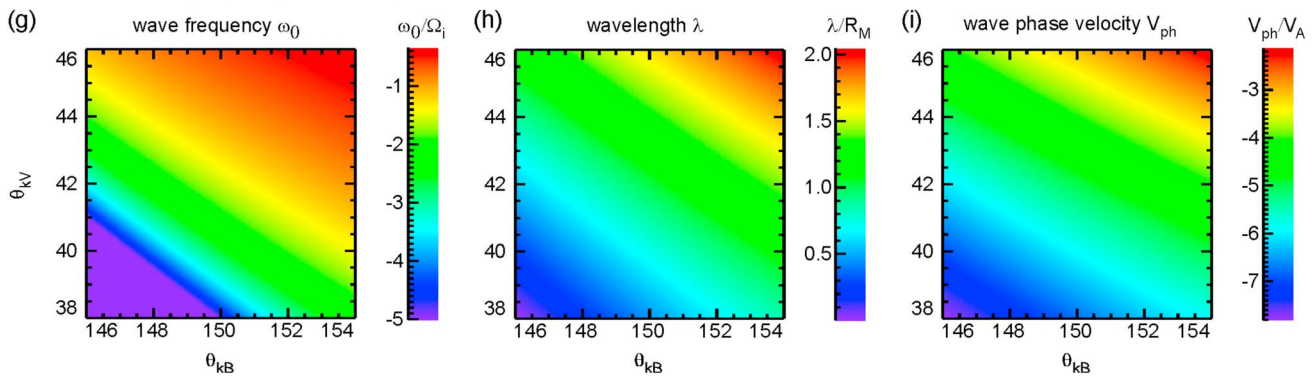
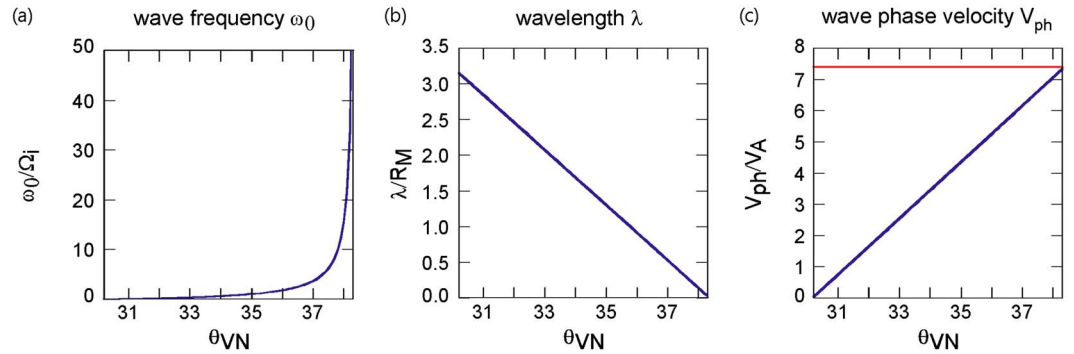


Figure 10. Sensitivity of the solutions of the newly born pickup ion generated waves to changes in θ_{kB} and θ_{kV} . The phase velocity depicted is normalized by the measured Alfvén velocity of 44 km/s. Only the first case, upstream propagating RH wave, has valid solutions for all the combinations of θ_{kB} and θ_{kV} . The latter two cases do not have valid solutions for any combination of θ_{kB} and θ_{kV} .

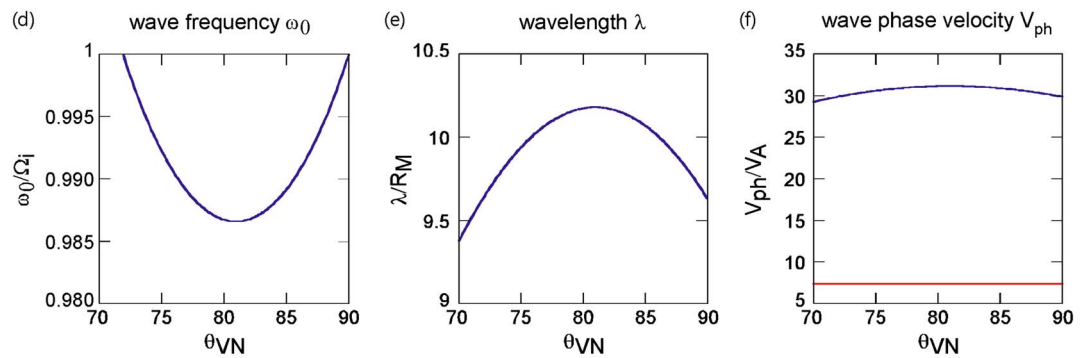
wave irrespective of its phase velocity because it is traveling downstream. Thus, there is no phase velocity restriction for this case and the only restrictions for this wave to be the observed wave are that f_0 and k should be positive. Using equations (1) and (2), as before, we find that $f_0 = -0.07$ Hz, $\lambda = 0.9 R_M$, and $V_{ph} = -232$ km/s, which is not a valid solution. Thus, the observed wave cannot be a left-hand polarized wave that propagates downstream.

It is interesting to determine the sensitivity of these solutions to the angles. For example, would the solution for the upstream propagating RH wave remain valid if θ_{kB} or θ_{kV} change by a small amount? To answer this, we find solutions to the above three cases varying θ_{kB} and θ_{kV} from their mean values by $\pm\Delta\theta$. These results are shown in Figure 10, and the case for the RH wave propagating upstream still continues to have valid solutions,

Upstream propagating RH wave parameters



Upstream propagating LH wave parameters



Downstream propagating LH wave parameters

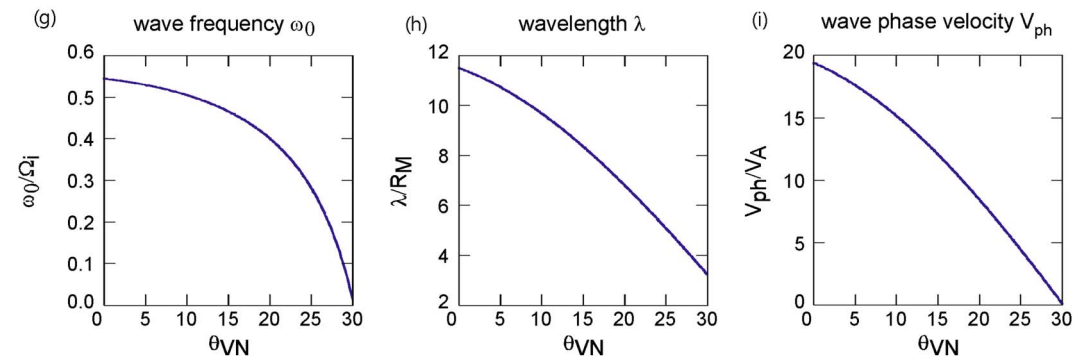


Figure 11. Valid solutions for the three cases of waves generated from the reflected solar wind ions at the bow shock. (c and f) The red lines mark the upper and lower limits for the wave phase velocity in order for the solutions to be valid. All the three cases for the wave have valid solutions but in different ranges of θ_{VN} .

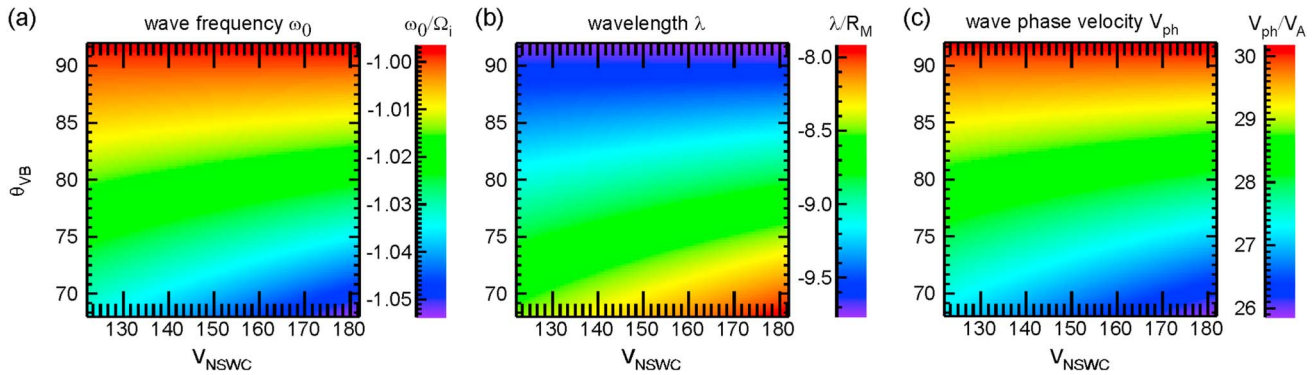
while the other two cases continue to have nonvalid solutions for all the combination of θ_{kB} and θ_{kV} that we consider. In particular, only the RH wave propagating upstream has positive values for frequency ($0 < \omega_0/\Omega_i < 5.1$), positive values for wavelength ($0 < \lambda/R_M < 2.1$), and positive values for phase velocity ($2 < V_{ph}/V_A < 8$).

4.2. Bow Shock Reflected Ion Generated Wave

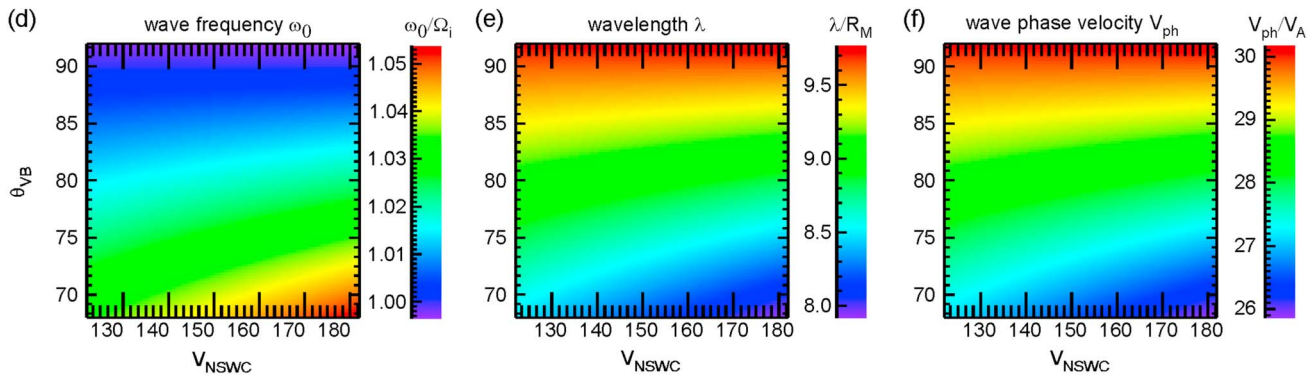
Now we consider the same three cases for the wave as with the newly born pickup ions. In this case, the ion beam velocity parallel to the magnetic field depends on θ_{VN} and the cone angle (Figures 7b and 8). As in section 4.1, we find solutions to the wave by imposing restrictions on f_0 , k , and V_{ph} . Here we search for valid solutions by varying θ_{VN} from 0° to 90° .

For the upstream propagating RH wave, we obtain valid solutions for $30^\circ < \theta_{VN} < 39^\circ$ (Figure 11a). For this case, the wavelength is less than $3 R_M$. For the upstream propagating LH wave, we obtain valid solutions for $70^\circ < \theta_{VN} < 90^\circ$ (Figure 11b). The waves corresponding to valid solutions have wavelengths between $9 R_M$

Upstream propagating RH wave parameters



Upstream propagating LH wave parameters



Downstream propagating LH wave parameters

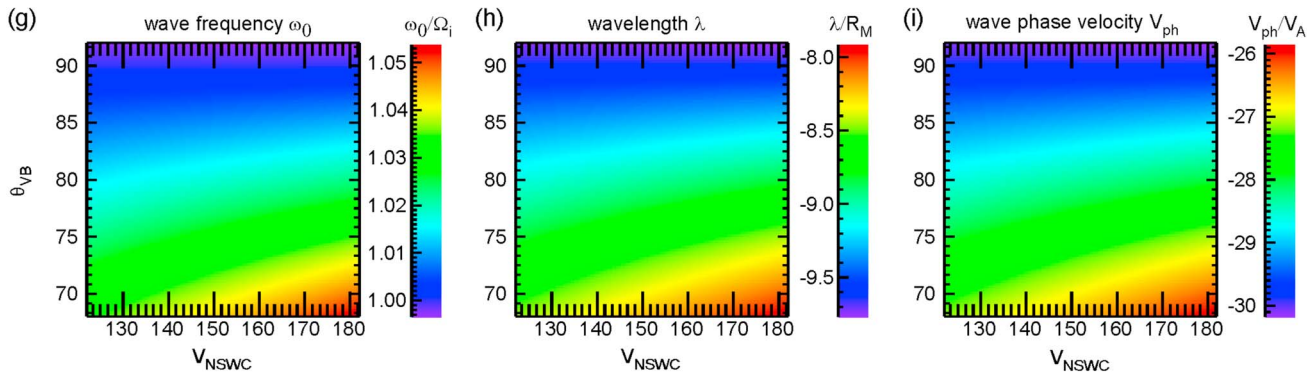


Figure 12. Sensitivity of the solutions of the NSWC generated waves to changes in NSWC parameters such as its velocity V_{NSWC} and angle between the velocity and the magnetic field θ_{VB} . Only the case for the upstream propagating LH wave has valid solutions.

and $10 R_M$. The downstream propagating LH wave, on the other hand, has valid solution for $0^\circ < \theta_{VN} < 30^\circ$ (Figure 11c). In this case the wavelengths corresponding to valid solutions have a much wider range: $3 R_M$ to $12 R_M$. Thus, if we assume specularly reflected solar wind ions from the bow shock, all the three cases for the wave become possibilities for the observed wave.

4.3. NSWC Generated Wave

By following a similar procedure for the above two ion sources, we find that only the upstream propagating LH wave has a valid solution (Figure 12). We obtain the same result when we account for the uncertainties of the wave parameters such as θ_{kB} , θ_{kV} , and the NSWC parameters such as the NSWC velocity V_{NSWC} , and the angle the NSWC velocity makes with the magnetic field θ_{VB} . The sensitivity of the solutions to V_{NSWC} and θ_{VB}

are shown in Figure 12. In particular, the upstream propagating RH wave has nonvalid solutions because the solutions have negative ω_0 and k (Figures 12a and 12b). The downstream propagating LH wave has nonvalid solutions because the solutions have negative k (Figure 12h).

5. Discussion

Out of the nine cases that we considered, only five cases are consistent with the observed wave: (i) newly born pickup ion generated upstream propagating RH wave; (ii) bow shock reflected ion generated upstream propagating RH wave; (iii) bow shock reflected ion generated upstream propagating LH wave; (iv) bow shock reflected ion generated downstream propagating LH wave; and (v) NSWC generated upstream propagating LH wave.

We can further discard some of these cases based on their wavelength. In particular, the latter three waves have very large wavelengths, greater than $3 R_M$. We can discard these large wavelength cases because they do not have sufficient time to grow into very large amplitudes. Using a one-dimensional hybrid simulation, Cowee *et al.* [2012] determined that the growth rate of pickup ion generated waves generally depend on the local ion production rate and the cone angle. Based on this simulation, they estimated that the waves travel a distance of $7 R_M$ to $119 R_M$ before saturating. As can be seen in Figure 1, the observed wave has very large amplitudes. Thus, we have just two possibilities for the wave: upstream propagating RH wave excited by newly born pickup ions or upstream propagating RH wave excited by reflected solar wind ions from the bow shock.

An important feature of a right-hand polarized wave is that it has correlated magnetic field and ion density fluctuations. Our observed wave has exactly this feature, where the ion density varies in phase with the magnetic field. This further strengthens our conclusion regarding the identity of the observed wave.

As discussed in section 3, the ion-density and the ion-temperature fluctuations are found to be anticorrelated. Such anticorrelation between electron temperature and density fluctuations was used by Thomsen *et al.* [1986] and Tsurutani *et al.* [1987] to distinguish upstream waves from viscous like subshocks. Since our wave also has this feature, upstream subshocks are not a possibility for our wave.

Another possibility for the observed wave that we have not considered here is ion cyclotron waves in the solar wind similar to those reported by Jian *et al.* [2009]. However, these waves tend to have frequencies larger than the local proton gyrofrequency in the spacecraft frame. Since the observed wave frequency is below the local proton gyrofrequency, we can discard this solar wind ion cyclotron wave possibility for the observed wave.

Lastly, we consider ion-ion nonresonant instabilities, which have zero frequency in the solar wind frame, i.e., $\omega_0 \approx 0$. However, their polarization can be either left or right handed [Gary, 2005]. Thus, using equation (2), we can determine the wavelength of such a wave using the observed wave parameters. In particular, $\lambda = 2\pi V_{sw} \cos(\theta_{KV}) / \omega_{sc}$. We obtain valid solutions, i.e., k positive, for an upstream propagating RH wave and a downstream propagating LH wave. However, both of these solutions have wavelengths larger than $3 R_M$. Thus, we can also discard the possibility of an ion-ion nonresonant instability.

We cannot conclusively determine the origin of the non-solar-wind component based on its composition and velocity. However, it should be either pickup ions or bow shock reflected pickup ions. The origin of the non-solar-wind component will be a subject of a future investigation. Pickup ions as well as reflected solar wind ions from the bow shock have been previously identified in the upstream regions of Mars [Barabash and Lundin, 1993; Yamauchi *et al.*, 2011, 2015; Rahmati *et al.*, 2015].

6. Summary

MAVEN observed a left-hand polarized wave which had very large fluctuations in the ion moments and magnetic field in the upstream region of Mars. A non-solar-wind component was also observed simultaneously with the wave. Including this non-solar-wind component, we considered three distinct ion sources that can be responsible for the wave generation. Using the measured wave parameters and the ambient plasma conditions, we determined that the most likely candidates for generation of the wave is either newly born pickup ions or reflected solar wind ions from the bow shock. We also determined that in the solar wind frame, the wave had a right-hand polarization and it propagated upstream. The wave was likely generated far upstream and grew to the large amplitude wave observed by MAVEN as the wave was convected downstream by the solar wind flow. The observed non-solar-wind component could have been merely perturbed by this large

amplitude wave. In our future work, we will use this approach to identify the ion sources responsible for the upstream waves at Mars. This will help us to determine the relative contributions from various ion sources to the upstream waves at Mars.

Acknowledgments

This work was supported by NASA and was partially supported by the CNES. MAVEN data are publicly available through the Planetary Data System.

References

- Barabash, S., and R. Lundin (1993), Reflected ions near Mars: PHOBOS-2 observations, *Geophys. Res. Lett.*, *20*, 787–790.
- Bertucci, C., C. Mazelle, and M. H. Acuña (2005), Interaction of the solar wind with Mars from Mars Global Surveyor MAG/ER observations, *J. Atmos. Sol. Terr. Phys.*, *67*, 1797–1808.
- Brain, D. A., F. Bagenal, M. H. Acuña, J. E. P. Connerney, D. H. Crider, C. Mazelle, D. L. Mitchell, and N. F. Ness (2002), Observations of low-frequency electromagnetic plasma waves upstream from the Martian shock, *J. Geophys. Res.*, *107*(A6), 1076, doi:10.1029/2000JA000416.
- Brinca, A. L., and B. T. Tsurutani (1987), Unusual characteristics of electromagnetic waves excited by newly born ions with large perpendicular energies, *Astron. Astrophys.*, *187*, 311–319.
- Brinca, A. L. (1996), Observation and interpretation of cometary low frequency waves, *Surv. Geophys.*, *17*, 1–39.
- Cattaneo, M. B. B., P. Cattaneo, G. Moreno, and R. P. Lepping (1991), Upstream waves in Saturn's foreshock, *Geophys. Res. Lett.*, *18*, 797–800.
- Connerney, J. E. P., J. Espley, P. Lawton, S. Murphy, J. Odom, R. Oliverson, and D. Sheppard (2015), The MAVEN magnetic field investigation, *Space Sci. Rev.*, 1–35, doi:10.1007/s11214-015-0169-4.
- Connerney, J. E. P., J. R. Espley, G. A. DiBraccio, J. R. Gruesbeck, R. J. Oliverson, D. L. Mitchell, J. Halekas, C. Mazelle, D. Brain, and B. M. Jakosky (2015), First results of the MAVEN magnetic field investigation, *Geophys. Res. Lett.*, *42*, 8819–8827, doi:10.1002/2015GL065366.
- Cowee, M. M., S. P. Gary, and H. Y. Wei (2012), Pickup ions and ion cyclotron wave amplitudes upstream of Mars: First results from the 1D hybrid simulation, *Geophys. Res. Lett.*, *39*, L08104, doi:10.1029/2012GL051313.
- Delva, M., C. Mazelle, and C. Bertucci (2011), Upstream ion cyclotron waves at Venus and Mars, *Space Sci. Rev.*, *162*, 5–24, doi:10.1007/s11214-011-9828-2.
- Gary, S. P. (2005), *Theory of Space Plasma Microinstabilities*, Cambridge Univ. Press, Cambridge, U. K.
- Goldstein, M. L., C. W. Smith, and W. H. Matthaeus (1983), Large amplitude MHD waves upstream of the Jovian bow shock, *J. Geophys. Res.*, *88*(A12), 9989–9999, doi:10.1029/JA088iA12p09989.
- Gosling, J. T., M. F. Thomsen, S. J. Bame, W. C. Feldman, G. Paschmann, and N. Sckopke (1982), Evidence for specularly reflected ions upstream from the quasi-parallel bow shock, *Geophys. Res. Lett.*, *9*, 1333–1336, doi:10.1029/GL009i012p01333.
- Halekas, J. S., A. R. Poppe, J. P. McFadden, and K.-H. Glassmeier (2013), The effects of reflected protons on the plasma environment of the moon for parallel interplanetary magnetic fields, *Geophys. Res. Lett.*, *40*, 4544–4548, doi:10.1002/grl.50892.
- Halekas, J. S., E. R. Taylor, G. Dalton, G. Johnson, D. W. Curtis, J. P. McFadden, D. L. Mitchell, R. P. Lin, and B. M. Jakosky (2013), The solar wind ion analyzer for MAVEN, *Space Sci. Rev.*, doi:10.1007/s11214-013-0029-z.
- Hoppe, M. M., C. T. Russell, L. A. Frank, T. E. Eastman, and E. W. Greenstadt (1981), Upstream hydromagnetic waves and their association with backstreaming ion populations: ISEE 1 and 2 observations, *J. Geophys. Res.*, *86*(A6), 4471–4492, doi:10.1029/JA086iA06p04471.
- Hoppe, M. M., and C. T. Russell (1983), Plasma rest frame frequencies and polarizations of the low-frequency upstream waves: ISEE 1 and 2 Observations, *J. Geophys. Res.*, *88*(A3), 2021–2027, doi:10.1029/JA088iA03p02021.
- Jian, L. K., C. T. Russell, J. G. Luhmann, R. J. Strangeway, J. S. Leisner, and A. B. Galvin (2009), Ion-cyclotron waves in the solar wind observed by STEREO near 1 AU, *Astrophys. J. Lett.*, *701*(2), L105–L109.
- Le, G., C. T. Russell, S. P. Gary, E. J. Smith, W. Riedler, and K. Schwingenschuh (1989), ULF waves at comets Halley and Giacobini-Zinner: Comparison with simulations, *J. Geophys. Res.*, *94*(A9), 11,989–11,995, doi:10.1029/JA094iA09p11989.
- Le, G., and C. T. Russell (1994), The morphology of ULF waves in the Earth's foreshock, in *Solar Wind Sources of Magnetospheric Ultra-Low-Frequency Waves*, edited by M. J. Engebretson, K. Takahashi, and M. Scholer, AGU, Washington, D. C., doi:10.1029/GM081p0075.
- Le, G., P. J. Chi, X. Blanco-Cano, S. Boardsen, J. A. Slavina, and B. J. Anderson (2013), Upstream ultra-low frequency waves in Mercury's foreshock region: MESSENGER magnetic field observations, *J. Geophys. Res. Space Physics*, *118*, 2809–2823, doi:10.1002/jgra.50342.
- Leisner, J. S., C. T. Russell, M. K. Dougherty, X. Blanco-Cano, R. J. Strangeway, and C. Bertucci (2006), Ion cyclotron waves in Saturn's E-ring: Initial Cassini observations, *Geophys. Res. Lett.*, *33*, L11101, doi:10.1029/2005GL024875.
- McFadden, J. P., et al. (2015), The MAVEN Suprathermal and thermal Ion Composition (STATIC) instrument, *Space Sci. Rev.*, *195*, 199–256.
- Mazelle, C., and F. M. Neubauer (1993), Discrete wave packets at the proton cyclotron frequency at comet P/Halley, *Geophys. Res. Lett.*, *20*, 153–156.
- Mazelle, C., et al. (2004), Bow shock and upstream phenomena at Mars, *Space Sci. Rev.*, *111*, 115–181.
- Orlowski, D. S., C. T. Russell, and R. P. Lepping (1992), Wave phenomena in the upstream region of Saturn, *J. Geophys. Res.*, *97*(A12), 19,187–19,199, doi:10.1029/92JA01461.
- Rahmati, A., D. E. Larson, T. E. Cravens, R. J. Lillis, P. A. Dunn, J. S. Halekas, J. E. Connerney, F. G. Eparvier, E. M. B. Thiemann, and B. M. Jakosky (2015), MAVEN insights into oxygen pickup ions at Mars, *Geophys. Res. Lett.*, *42*, 8870–8876, doi:10.1002/2015GL065262.
- Romanelli, N., C. Bertucci, D. Gómez, C. Mazelle, and M. Delva (2013), Proton cyclotron waves upstream from Mars: Observations from Mars Global Surveyor, *Planet. Space Sci.*, *76*, 1–9.
- Ruhunusiri, S., J. S. Halekas, J. E. P. Connerney, J. R. Espley, J. P. McFadden, D. E. Larson, D. L. Mitchell, C. Mazelle, and B. M. Jakosky (2015), Low-frequency waves in the Martian magnetosphere and their response to upstream solar wind driving conditions, *Geophys. Res. Lett.*, *42*, 8917–8924, doi:10.1002/2015GL064968.
- Russell, C. T., J. G. Luhmann, K. Schwingenschuh, W. Riedler, and Ye. Yeroshenko (1990), Upstream waves at Mars: Phobos observations, *Geophys. Res. Lett.*, *17*, 897–900.
- Russell, C. T., R. P. Lepping, and C. W. Smith (1990), Upstream waves at Uranus, *J. Geophys. Res.*, *95*(A3), 2273–2279, doi:10.1029/JA095iA03p02273.
- Russell, C. T. (1994), Planetary upstream waves, in *Solar Wind Sources of Magnetospheric Ultra-Low-Frequency Waves*, edited by M. J. Engebretson, K. Takahashi, and M. Scholer, AGU, Washington, D. C., doi:10.1029/GM081p0075.
- Russell, C. T., X. Blanco-Cano, Y. L. Wang, and M. G. Kivelson (2003), Ion cyclotron waves at Io: Implications for the temporal variation of Io's atmosphere, *Planet. Space Sci.*, *51*, 937–944.
- Russell, C. T., S. S. Mayerberger, and X. Blanco-Cano (2006), Proton cyclotron waves at Mars and Venus, *Adv. Space Res.*, *38*, 745–751.
- Smith, C. W., M. L. Goldstein, and W. H. Matthaeus (1983), Turbulence analysis of the Jovian upstream 'wave' phenomenon, *J. Geophys. Res.*, *88*(A7), 5581–5593, doi:10.1029/JA088iA07p05581.

- Tan, L. C., G. M. Mason, and B. T. Tsurutani (1993), Evidence for proton cyclotron waves near comet Giacobini-Zinner, *Geophys. Res. Lett.*, *20*(3), 169–172.
- Thomsen, M. F., S. J. Bame, W. C. Feldman, J. T. Gosling, D. J. McComas, and D. T. Young (1986), The comet/solar wind transition region at Giacobini-Zinner, *Geophys. Res. Lett.*, *13*, 393–396.
- Thorne, R. M., and B. T. Tsurutani (1987), Resonant interactions between cometary pickup ions and low frequency electromagnetic waves, *Planet. Space Sci.*, *35*, 1501–1511.
- Trotignon, J., C. Mazelle, C. Bertucci, and M. Acuña (2006), Martian shock and magnetic pile-up boundary positions and shapes determined from the Phobos 2 and Mars Global Surveyor data sets, *Planet. Space Sci.*, *54*(4), 357–369, doi:10.1016/j.pss.2006.01.003.
- Tsurutani, B. T., and E. J. Smith (1986), Hydromagnetic waves and instabilities associated with cometary pickup: ICE observations, *Geophys. Res. Lett.*, *13*, 263–266.
- Tsurutani, B. T., R. M. Thorne, E. J. Smith, J. T. Gosling, and H. Matsumoto (1987), Steepened magnetosonic waves at comet Giacobini-Zinner, *J. Geophys. Res.*, *92*(A10), 11,074–11,082, doi:10.1029/JA092iA10p11074.
- Tsurutani, B. T., D. J. Southwood, E. J. Smith, and A. Balogh (1993), A survey of low frequency waves at Jupiter: The Ulysses encounter, *J. Geophys. Res.*, *98*(A12), 21,203–21,216, doi:10.1029/93JA02586.
- Warnecke, J., M. G. Kivelson, K. K. Khurana, D. E. Huddleston, and C. T. Russell (1997), Ion cyclotron waves observed at Galileo's Io encounter: Implications for neutral cloud distribution and plasma composition, *Geophys. Res. Lett.*, *24*, 2139–2142.
- Wei, H. Y., and C. T. Russell (2006), Proton cyclotron waves at Mars: Exosphere structure and evidence for a fast neutral disk, *Geophys. Res. Lett.*, *33*, L23103, doi:10.1029/2006GL026244.
- Wei, H. Y., C. T. Russell, T. L. Zhang, and X. Blanco-Cano (2011), Comparative study of ion cyclotron waves at Mars, Venus and Earth, *Planet. Space Sci.*, *59*, 1039–1047.
- Wei, H. Y., M. M. Cowee, C. T. Russell, and H. K. Leinweber (2014), Ion cyclotron waves at Mars: Occurrence and wave properties, *J. Geophys. Res. Space Physics*, *119*, 5244–5258, doi:10.1002/2014JA020067.
- Zhang, M., J. W. Belcher, J. D. Richardson, V. M. Vasyliunas, R. P. Lepping, N. F. Ness, and C. W. Smith (1991), Low-frequency waves in the solar wind near Neptune, *Geophys. Res. Lett.*, *18*, 1071–1074.
- Yamauchi, M., et al. (2011), Comparison of accelerated ion populations observed upstream of the bow shocks at Venus and Mars, *Ann. Geophys.*, *29*, 511–528.
- Yamauchi, M., et al. (2015), Seasonal variation of Martian pick-up ions: Evidence of breathing exosphere, *Planet. Space Sci.*, doi:10.1016/j.pss.2015.09.013.